

Aviation Fuel Cavitation in a CD Nozzle: A Quantitative Experimental Characterization⁺

¹Michael Waldrop*, ¹Flint Thomas**

¹*Institute for Flow Physics and Control, University of Notre Dame, Notre Dame, IN, USA*

Abstract

This work describes experiments aimed at clarifying several physical aspects of aviation fuel cavitation. The experiments are performed in a simple two-dimensional converging-diverging (CD) nozzle geometry with JP-8 fuel replaced by dodecane, a single component surrogate and its primary component by weight. Experiments are focused on gaseous cavitation with air micro-bubbles injected at the nozzle inlet. Carefully controlled initial void fraction leads to bubble growth in the bulk of the fluid and quasi-1D flow patterns downstream. These experiments seek to characterize the flow patterns with particular focus on propagating shock waves that form due to collapse of gaseous bubble clouds. Experimental documentation is made through arrays of static and unsteady pressure sensors, high-speed video and a volumetric flow rate meter. The results are analyzed to obtain choked mass flow rate, distributions of mean streamwise pressure, shock propagation speed, local shock passage frequency, and static pressure jump across the bubbly shock.

Keywords: Cavitation, Bubbly Shocks, Shockwaves, Bubbly Flows, Aviation Fuel

Introduction and Motivation

The occurrence of cavitation in an aircraft fuel system can lead to unexpected degradation in system performance and damage to fuel system components. JP-8 aircraft fuel has been shown to be prone to cavitation in piston fuel pumps and other system components which motivates this experimental examination. Several previous studies of cavitation in jet fuel have been made in order to more fully understand its behavior. Notable among these is the work of Dunn et al.¹ which examines cavitating, choked CD nozzle flows of JP-8 fuel, dodecane and water in comparison to predictions of a barotropic cavitation model. Their results show that, for flows with or without inlet air injection, a standing shock exists in the diverging portion of the nozzle for water and a significantly milder shock (over larger streamwise region) exists for dodecane. Meanwhile, JP-8 exhibits no shock behavior but instead shows a more gradual pressure rise from its minimum near the nozzle throat to the outlet pressure. The shock location changes with variation in back pressure as well as changes in initial void fraction for the air-injected case. Dunn et al.¹ attribute the differences between the choked, cavitating CD nozzle flows of water, dodecane and JP-8 to differences in their respective fluid properties, primarily surface tension and viscosity. These results are intriguing but do not encapsulate the full range of behaviors predicted by numerical modelling. For example, the work of Preston et al.² describes two additional cavitation regimes for flows with controlled initial void fraction. These are an unsteady regime with propagating shock waves in the diverging portion of the nozzle and a steady but underexpanded regime at extremely low back pressure. Experimental exploration of these regimes has been minimal in water, jet fuel or any other fluid. Their study in JP-8 is greatly aided by replacing the fuel with dodecane, its largest component by weight³, as a single-component surrogate. JP-8 contains more than 200 hydrocarbons³ in varying ratios from sample to sample. As a result, properties of the fuel are often not repeatable and the reliability of dodecane is preferable for scientific study. For this reason, the experiments described herein utilize dodecane-air mixtures to examine gaseous cavitation in aviation fuel. A simple, effectively two-dimensional CD nozzle geometry provides a pressure drop sufficient to induce cavitation in these mixtures and permits thorough study of propagating bubbly shock waves in the resulting flows.

Experimental Apparatus

A conceptual schematic of the experimental facility is shown in Figure 1(a). Flow is driven through a vertically oriented, Plexiglas™ CD nozzle by pressure differential between an upstream tank open to atmosphere and an evacuated downstream vacuum tank. The volumetric flow rate of liquid entering the nozzle is measured with Dwyer's™ TVF-02 Industrial Flow Meter. An infusion pump supplies air at either of two distinct rates to a pair of

⁺Work funded by Honeywell Aerospace

*Michael Waldrop: mwaldrop@nd.edu

**Flint Thomas: fthomas@nd.edu

33 gauge, blunt tip hypodermic needles at the nozzle inlet as shown schematically in Figure 1(b). The first infusion rate (0.429 mL/s) equates to an initial void fraction (α_0) of $\sim 1.1\%$ for dodecane in choked flow while the second rate (0.176 mL/s) gives $\alpha_0 \sim 0.47\%$ under the same conditions. Figure 1(c) is a conceptual schematic of the high-speed imaging process. The test section is backlit from a distance of 1.83 m with a theater lamp. A translucent plastic diffuser is placed immediately behind the test section while the lens of a Photron FASTCAM™ SA1.1 high-speed camera is positioned 0.6 m away. This technique causes the liquid phase to appear bright in the resulting images while the gas/vapor phase is dark. Average pressure measurement is performed with a streamwise array of 40 static pressure taps evenly spaced along the centerline of the nozzle and a set of four Setra™ Model 209 vacuum pressure transducers. Unsteady pressure measurement is achieved with four Measurement Specialties™ EPIH-37B absolute pressure transducers that may be placed at any point along the nozzle centerline. The pressure taps for average pressure measurements and the set of unsteady pressure transducers are each mounted in one several interchangeable, Plexiglas™ face plates that act as one of the CD nozzle walls. Another face plate, free of any pressure measurement apparatus but marked with fiduciary indicators every 1.27 cm along the nozzle length is used for high-speed imaging. With this setup shock propagation speed can be accurately determined.

The symmetric CD nozzle used for this investigation (shown in Figure 2) has a rectangular cross section, length (L) of 0.127 m and constant depth (d) of 0.1588 cm. The converging portion is 2.54 cm in length while the diverging portion is 9.525 cm long. The intervening 0.635 cm section consists of a constant area throat with height of 0.1588 cm. The nozzle inlet and outlet are each 1.905 cm in height. Both the converging and diverging section contours are defined by fifth order polynomials with zero first and second derivative end conditions.

Results and Analysis

Experimental characterization of gaseous dodecane cavitation begins with measurements of mean streamwise static pressure distribution and mass flow rates for a broad range of nozzle pressure ratios. These results are presented in Figure 2 which shows the mean pressure at all forty static tap locations across the indicated range of nozzle back pressure to inlet pressure (P_B/P_0) ratios. Curves with $P_B/P_0 < 0.5$ are indicative of choked nozzle flow as all curves follow the same path through the nozzle throat and measured mass flow rate is identical for each case ($\dot{m}_c = 0.0261$ kg/s, see Table 1). These curves also show a sharp rise in static pressure over a small spatial region, consistent with the presence of a normal shock in the diverging section. As described later, each of these cases also exhibits unsteady shock waves propagating downstream in high-speed video imaging. Higher pressure ratio cases ($0.58 < P_B/P_0 < 0.8$) do not follow the same path through the throat and show a variable mass flow rate indicating unchoked flow.

The time mean pressure distributions are useful in describing the broad properties of the flow but provide little insight into the inherently unsteady mechanisms associated with shock formation and propagation. Such phenomena are more easily studied through the use of high-speed video. High-speed imaging is first used to study the properties of air micro bubbles injected at the nozzle inlet as depicted in Figure 3. Mean bubble injection frequency is measured via the number of bubbles passing a fiduciary marker over the duration of a high-speed video image sequence. The diameter of an individual injected bubble is then obtained by counting the number of pixels across its widest dimension and using the number of pixels between fiduciary markers to convert to physical units. An average of the first 20 bubbles to cross the fiduciary marker is then recorded as the mean initial bubble diameter. Injection frequencies and mean initial bubble diameters for air injected into dodecane may be found in Table 2. As shown in the sample image in Figure 3, injected bubbles initiate cavitation in the fluid bulk near the nozzle throat which results in clouds of gaseous bubbles downstream. These clouds are found to undergo collapse and emit planar shock waves which propagate downstream from the collapse location. High-speed images of these shocks are examined for emission frequency, average propagation speed across the nozzle and formation location utilizing the time derivative of pixel saturation between subsequent images. As previously discussed, regions with high pixel saturation are associated with the liquid phase while darker pixels indicate a gaseous void. These voids tend to reduce in size under the pressure jump associated with a passing shock wave, meaning regions with a positive time derivative of pixel saturation between subsequent frames indicate a passing shock. After using a spatial Butterworth filter to remove small scale phenomena and applying a color scale to the derivative images, the shock waves appear

⁺Work funded by Honeywell Aerospace

*Michael Waldrop: mwaldrop@nd.edu

**Flint Thomas: fthomas@nd.edu

as blue regions and may be tracked between images as shown in Figure 4. This, along with the fiduciary markers in the high-speed images, permits measurement of shock speed, emission frequency and emission location.

Histograms of shock emission frequency, average shock speed and emission location have been obtained from the video imaging and may be found in Figure 5. Shocks are emitted across a fairly narrow streamwise band with $0.45 \leq (x/L)_E \leq 0.55$. This coincides with the region of sharp increases in mean static pressure for the choked flow cases shown in Figure 2. Emission frequency and propagation speed show some evidence of bimodality but confirmation requires acquisition of additional samples in order to refine the statistics. Unsteady pressure measurements provide significantly more data, allowing for verification of shock emission frequency results as well as determination of a typical shock pressure profile at a given x/L location. With unsteady pressure sensors placed at “Unsteady Pressure Tap Array” locations 1,3,4 and 5 (see Figure 2) 20 seconds of pressure time-series data sampled at 102.4 kHz yields fully converged shock statistics and a well-defined typical shock pressure distribution shape for each sensor. The arrival of a shock is determined by a sudden jump in pressure above a specified threshold for a specified duration (span). Threshold and span values are unique to each sensor and each sampling run. They are determined by comparison to a visual count of shock events in the raw pressure signal (number of shock events in first 20,000 samples). Once threshold and span are determined, frequency of shocks and their average pressure signature may be obtained.

Figure 6 shows histograms of time between shock arrivals (Figure 6(a)) and shock arrival frequency (Figure 6(b)) at Sensor 4 ($x/L=0.9$) in a dodecane-air flow with $P_B/P_0=0.36$ and $\alpha_0 = 1.1\%$. They are normalized by the average time between bubble injections and average frequency of bubble injections, respectively (see Table 1). These confirm the bimodal nature of the shock emissions hinted at by the derivative image technique and show that each of these modes occurs at a harmonic of the bubble injection frequency. This is a strong indicator that shock emission in this flow is directly driven by air micro bubble injection.

Figure 7 shows typical shock pressure profiles obtained by averaging all the shock events identified in the raw pressure signal from each sensor. Figure 7(a) demonstrates the reduction in pressure jump magnitude of a typical shock as it propagates downstream. A 36.6 kPa jump in pressure occurs at $x/L=0.5$ while 12.6 kPa, 9.5 kPa and 8.8 kPa pressure jumps occur at $x/L=0.8, 0.9$ and 1.0 respectively. Figure 7(a) also demonstrates that pre and post-shock pressures are significantly lower at $x/L = 0.5$ (12.6 kPa pre-shock and 17.9 kPa post-shock) than $x/L = 0.8, 0.9$ and 1.0 . These pressures are effectively identical between the sensors farther downstream (~ 26 kPa pre-shock and ~ 29 kPa post shock). This is consistent with the essentially constant average pressure in this region for the $P_B/P_0=0.36$ case shown in Figure 2. Figures 7(b) and 7(c) show the typical pressure signal from three different data runs normalized by their respective maximum values. The resulting curves are effectively identical and confirm the repeatability of the typical shock shape at a given streamwise location.

Figures & Tables:

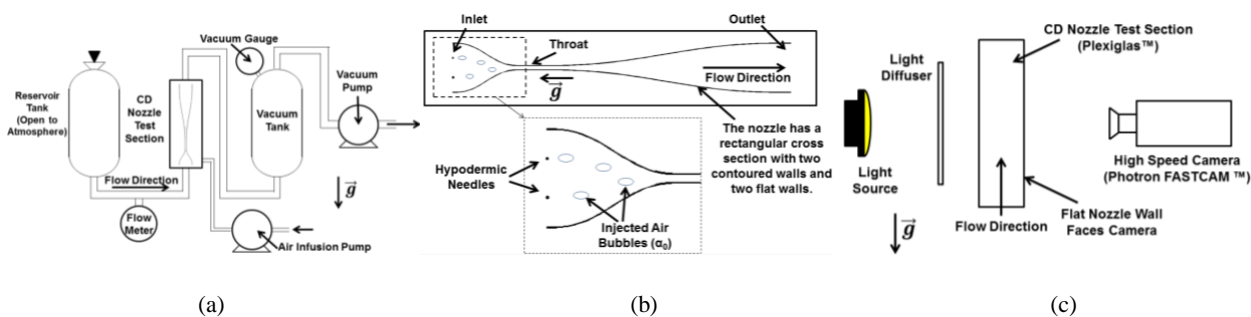


Figure 1: (a) Cavitation facility, (b) micro-bubble injection method, (c) high-speed imaging technique

⁺Work funded by Honeywell Aerospace
 *Michael Waldrop: mwaldrop@nd.edu
 **Flint Thomas: fthomas@nd.edu

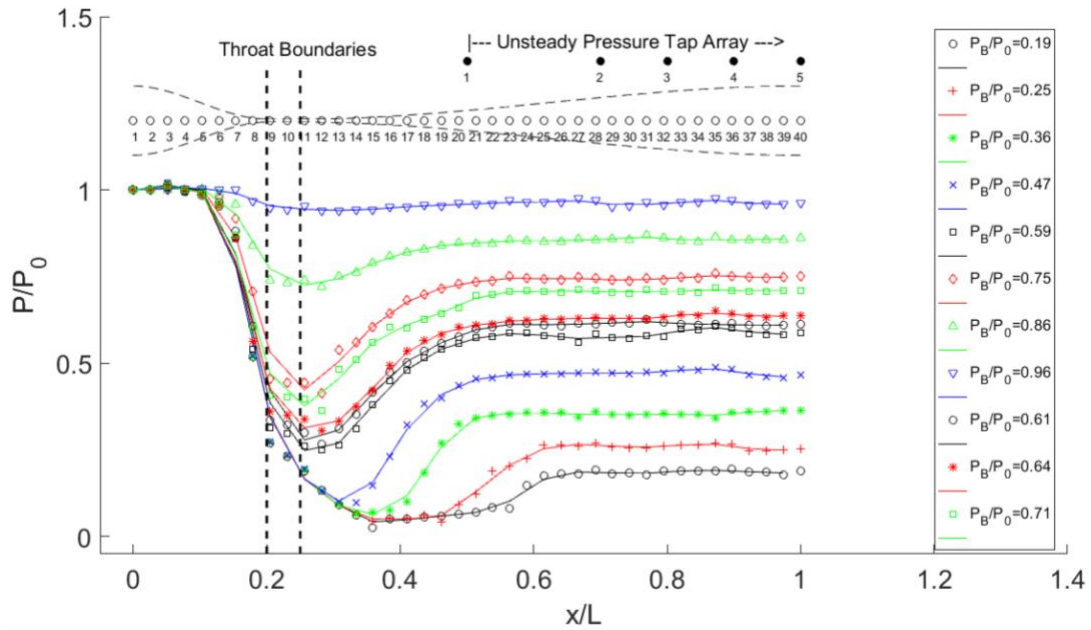


Figure 2: Average pressure distribution for gaseous cavitation of dodecane and injected air ($\alpha_0 = 1.1\%$) in a CD nozzle at various back pressure ratios with nozzle profile and pressure tap configurations

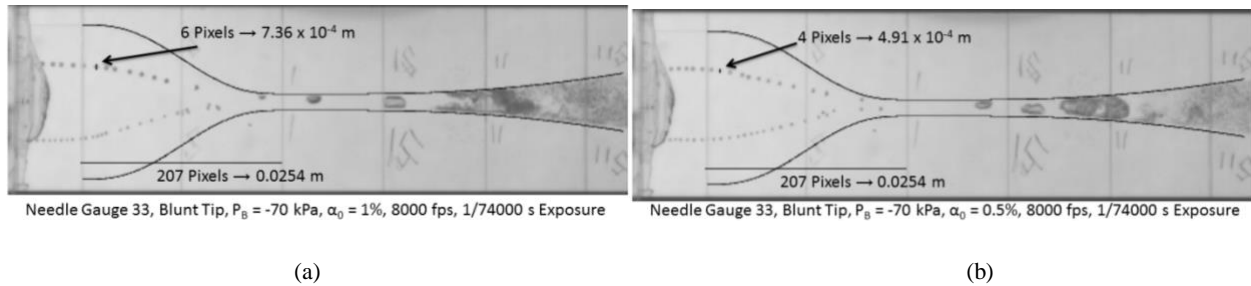


Figure 3: Sample high-speed video images of air micro-bubble injection frequency and diameter for (a) $\alpha_0 = 1.1\%$ and (b) $\alpha_0 = 0.47\%$

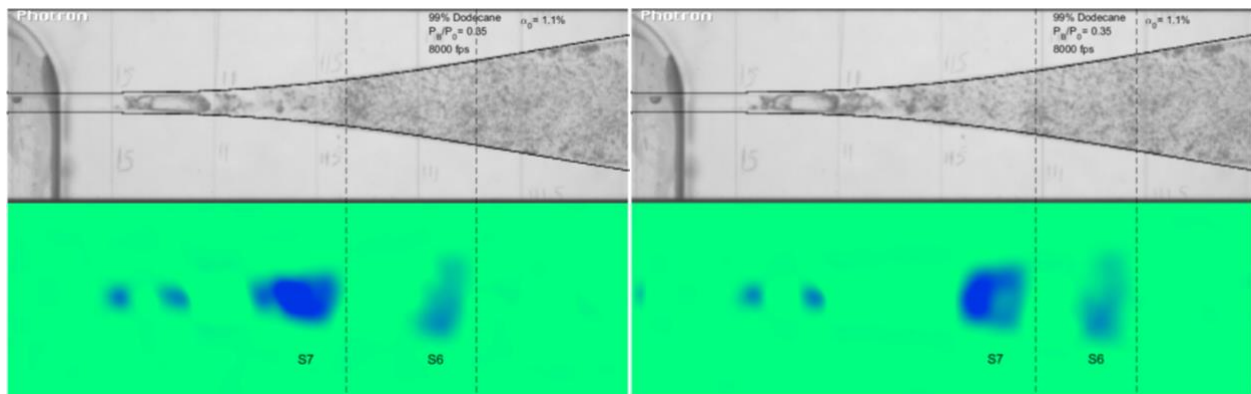


Figure 4: Shock propagation due to gaseous cavitation in micro air bubble injected dodecane flow through a CD nozzle ($P_B/P_0 = 0.36$ and $\alpha_0 = 1.1\%$). (Blue regions are indicative of propagating shock waves.)

+Work funded by Honeywell Aerospace
 *Michael Waldrop: mwaldrop@nd.edu
 **Flint Thomas: fthomas@nd.edu

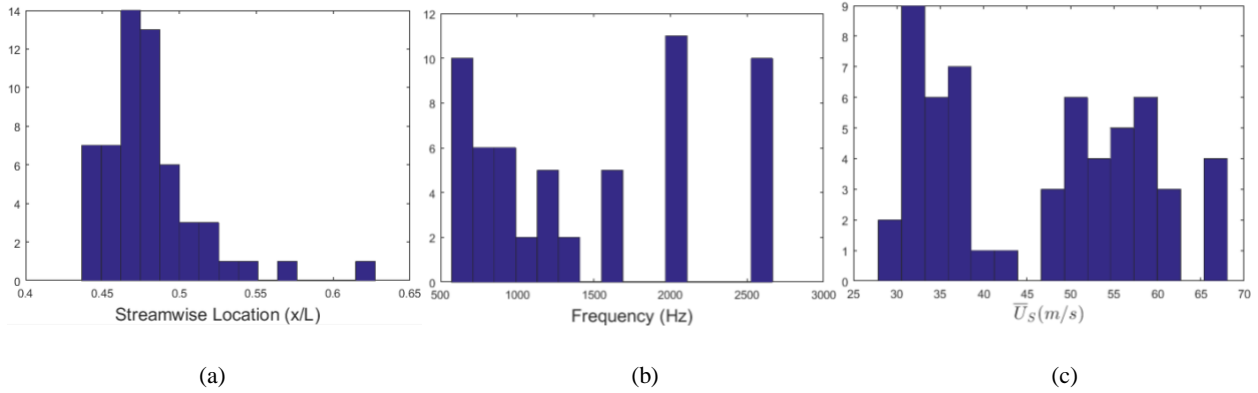


Figure 5: High-speed video derived histograms of shock waves due to gaseous cavitation in micro air bubble injected dodecane flow through a CD nozzle ($P_B/P_0=0.36$ and $\alpha_0 = 1.1\%$): (a) emission location, (b) emission frequency and (c) propagation speed

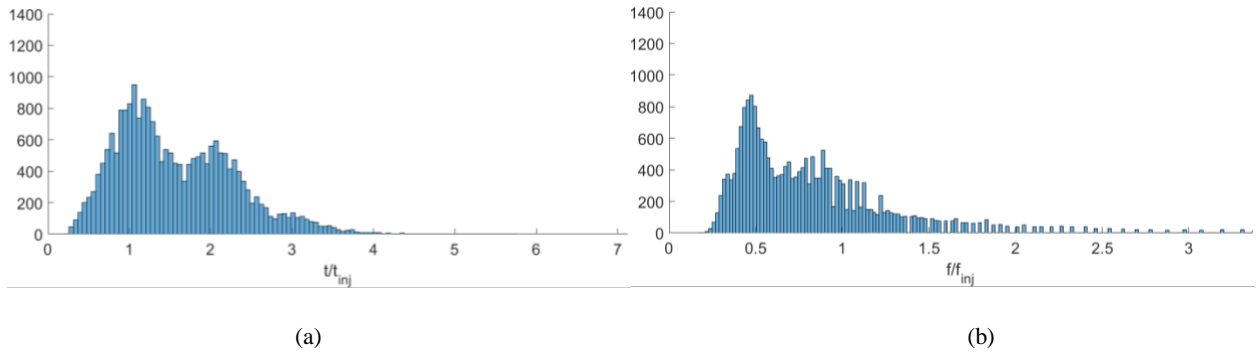


Figure 6: Unsteady pressure derived histograms of shocks due to gaseous cavitation in micro air bubble injected dodecane flow through a CD nozzle ($P_B/P_0=0.36$ and $\alpha_0 = 1.1\%$): (a) time between shocks normalized by average time between bubble injections, (b) shock emission frequency normalized by average bubble injection frequency

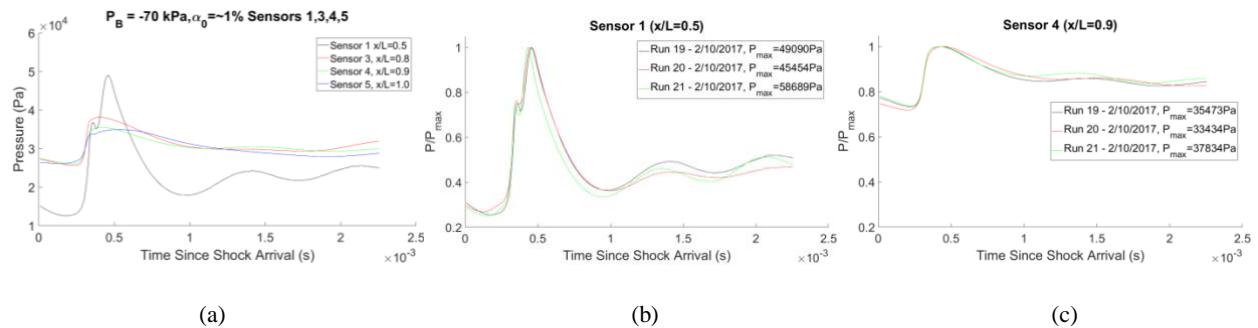


Figure 7: Gaseous cavitation induced shock pressure profiles in micro air bubble injected dodecane flow through a CD nozzle ($P_B/P_0=0.36$ and $\alpha_0 = 1.1\%$): (a) various x/L locations for a single sampling run, multiple sampling runs normalized to local max shock pressure at (b) $x/L=0.5$ and (c) $x/L=0.9$

⁺Work funded by Honeywell Aerospace
^{*}Michael Waldrop: mwaldrop@nd.edu
^{**}Flint Thomas: ftthomas@nd.edu

P_B/P_0	α_0	Mass Flow Rate (kg/s)	Bubble Count (Over Full Video)	Injection Frequency (Hz)	Average Initial Bubble Diameter (Pixels)	Average Initial Bubble Diameter (m)
0.19	1.1%	0.0261	127	1227	6.7	7.4×10^{-4}
0.25	1.1%	0.0261	126	1217	6.6	7.4×10^{-4}
0.36	1.1%	0.0261	123	1188	6.35	7.1×10^{-4}
0.47	1.1%	0.0261	133	1285	6	6.68×10^{-4}

Table 1: Inlet bubble properties and critical flow properties for gaseous cavitation of dodecane and injected air in a CD nozzle

Conclusion

Gaseous cavitation in aviation fuel is examined through the use of dodecane-air mixtures in flows through a converging-diverging nozzle where dodecane serves as a single component fuel surrogate. Cavitation induced choked flow occurs in the nozzle for back pressure ratios of 0.5 or less with a choked mass flow rate of 0.0261 kg/s and choked throat pressure ratio of 0.23. High-speed video and unsteady pressure measurements show that for gaseous cavitation due to injection of air micro bubbles at the CD nozzle inlet (1.1 % initial void fraction, 0.36 back pressure ratio) there is a bimodal distribution of shock emission frequency and propagation speed in the diverging portion of the nozzle. Shock emission location is fairly localized ($0.45 \leq (x/L)_E \leq 0.55$) for this case. Unsteady pressure data shows the two modes of shock emission frequency occur at harmonics of the air micro bubble injection frequency. This is a strong indicator that bubbly shock emission in the nozzle's diverging portion is driven by bubble injection at the nozzle inlet. This data is also used to characterize the pressure signature of a typical shock wave as it passes each pressure sensor. The magnitude of pressure jump across the shock decreases as it propagates downstream (36.6 kPa at $x/L=0.5$, ~10 kPa closer to the outlet) and the background pressures pre and post-shock are significantly lower at $x/L=0.5$ (12.6 kPa and 17.9 kPa respectively) than at sensors downstream. Pre-shock pressure and post-shock pressure are greater in magnitude and effectively unchanged between sensors at $x/L = 0.8, 0.9$ and 1.0 (~26 kPa and ~29 kPa respectively). Typical shock shapes are also shown to be consistent between sampling runs for a given streamwise location when normalized by their respective maximum pressures. These findings demonstrate that an understanding of the distribution of extant bubbles in a fuel system and the effect of the flow geometry on individual bubbles can be used to predict the frequency and magnitude of shocks downstream of a cavitation event. This knowledge could be used to significantly mitigate any damage cavitation might cause to fuel system components.

References

- [1] Dunn, P., Thomas, F., Davis, M., & Dorofeeva, I. (2010). *Experimental Characterization of Aviation-Fuel Cavitation*. *Physics of Fluids*. 22,117102.
- [2] Preston, A. T., Colonius, T., & Brennen, C. E. (2002). *A Numerical Investigation of Unsteady Bubbly Cavitating Nozzle Flows*. *Physics of Fluids*, 14(1), 300-311.
- [3] *Handbook of Aviation Fuel Properties*, 2004, 3rd Ed., Coordinating Research Council, Inc.

⁺Work funded by Honeywell Aerospace

*Michael Waldrop: mwaldrop@nd.edu

**Flint Thomas: fthomas@nd.edu